Robust phenotypic plasticity of symbiotic organs facilitates the adaptation and evolution of deep-sea mussels

Mengna Li[1,3,4,5], Hao Chen[1,3,4*], Minxiao Wang[1,3,4], Zhaoshan Zhong[1,3,4], Chao Lian[1,3,4], Li Zhou[1,3,4], Huan Zhang[1,3,4], Hao Wang[1,3,4], Lei Cao[1,3,4], Chaolun Li[1,2,3,4,5*]

[1] Center of Deep Sea Research, and CAS Key Laboratory of Marine Ecology and Environmental Sciences, Institute of Oceanology, Chinese Academy of Sciences, Qingdao 266071, China.

[2] South China Sea Institute of Oceanology, Chinese Academy of Sciences, Guangzhou 510301, China.

[3] Laboratory for Marine Ecology and Environmental Science, Qingdao National Laboratory for Marine Science and Technology, Qingdao 266071, China.

[4] Center for Ocean Mega-Science, Chinese Academy of Sciences, Qingdao 266071, China.

[5] University of Chinese Academy of Sciences, Beijing 10049, China.

*Corresponding author. Email: chenhao@qdio.ac.cn (H.C.), lcl@qdio.ac.cn (C.L.)

Abstract

Phenotypic plasticity and symbiosis are two key factors influencing the evolution and adaptation. However, knowledge of how symbiotic cells and organs evolve under and adapt to emerging environmental changes is still scarce. Herein, we assessed the long-term phenotypic changes of gill in aposymbiotic deep-sea mussels induced by methane deprivation to clarify the physiological basis that facilitates evolution and adaptation of mussels. We showed that aposymbiotic mussels managed a long survival by digesting symbionts and remodeling the global metabolism to conserve energy. The mussels also replaced bacteriocytes with ciliated cells to support filter-feeding, and retained robust generation of new cells to dynamically respond to

environmental changes. These phenotypic changes were regulated by sterol-related signaling pathway of host and influenced by sterol metabolism of symbiont. The robust plasticity of gill advantages the evolution and adaptation of deep-sea mussels, and highlights the interaction between environment and symbiosis in the complex evolution of holobionts.

Introduction

Phenotypic plasticity, which allows organisms to alter their physiology, development, morphology, or behavior in response to environmental signals, is implicated as a major factor influencing the evolution of eukaryotes[1]. Symbiosis is suggested to be a direct outcome of phenotypic plasticity and a source of phenotypic polymorphism that has substantially expanded the ecological ranges of organisms via the mutualistic interaction with symbionts[2]. While the breadth and importance of symbiosis and phenotypic plasticity are well recognized, the interaction between phenotypic plasticity and symbiosis, including how plasticity has facilitated the acquisition of symbiotic traits and how symbiotic associations reciprocally influence phenotypes, are yet to be fully elucidated[3]. With a growing body of information obtained from model holobionts, such as the Hawaiian bobtail squid (*Euprymna scolopes*) and hemimetabolous aphids, the formation and maturation processes of symbiotic cells and organs, as the core trait of symbiosis, are now becoming clear[4]. Research has shown that the acquisition of symbiotic cells and organs can be facilitated by a set of conserved molecules and modulated by symbionts[5–7]. However, knowledge of how hosts maintain the proper function and development of symbiotic cells and organs under emerging environmental changes and how the symbionts influence these processes remained to be elucidated, which further hinders the understanding of evolution and adaptation of symbiosis.

The Mollusca phylum is the second most species-rich phylum, with a wide range of habitats including fresh water, intertidal regions, and even the deep sea. In addition to their vast diversity of body plans, mollusks are also known to possess diverse and intimate symbiotic associations with microbes that allow them to obtain nutrition[8].

Studies have further shown that the symbiotic associations between mollusks and microbes can vary with regard to the location of symbionts and their type and transmission mode[9]. Moreover, the mollusk holobionts have benefited greatly from the diverse symbiotic associations by expanding their habitats and biomass in almost all marine ecosystems, from shallow-water seagrass beds to deep-sea hydrothermal vents and cold seeps. It has been estimated that the symbiotic association in mollusks was established only a few hundred million years ago, after which the mollusk holobionts have evolved multiple times to adapt to new environments[10,11]. Symbiotic associations may even have been lost in some deep-sea mussels during periods when organic matter was more accessible[12]. The diverse and dynamic changes of symbiotic traits therefore make bivalves promising models for the investigation of the evolution and adaptation of symbiotic associations.

As endemic species in deep-sea cold seeps and hydrothermal vents, deep-sea mussels are known to harbor methanotrophs and/or thiotrophs in their specialized gill epithelial cells (bacteriocytes) as their major source of nutrition[8]. Deep-sea mussels can obtain these symbionts horizontally from the environment throughout their life spans[13]. Biogeography research has shown that deep-sea mussels are usually distributed in patches close to fluid flows or seepages with high concentrations of methane or sulfides to maximize the fitness of symbiotic association[14]. Nevertheless, some deep-sea mussels are also found in regions with insufficient methane or sulfides, and can regain their symbiotic association even when the symbionts are completely lost due to the deprivation of these chemicals[15], providing a unique opportunity to investigate the environmental influence on symbiotic associations and the phenotypic changes of symbiotic traits in relation to different symbiotic states. Therefore, this study conducted a long-term methane deprivation assay on the methanotrophic deep-sea mussel (*Gigantidas platifrons*) to assess the dynamic changes of symbiotic cells and organs during methane deprivation and symbiont depletion. Using multi-omics analysis, the molecular basis underlying the dynamic phenotypic changes was decoded. Finally, by comparing data obtained from symbiotic and decolonized mussels, this study addressed the possible influences of symbionts in the phenotypic

changes of symbiotic cells and organs.

Results

Phenotypic changes of symbiotic organs under methane deprivation

To assess the phenotypic changes of the symbiotic cells and organs of deep-sea mussels under long-term methane deprivation, a laboratory recirculating system was set up to cultivate the methanotrophic *G. platifrons* mussels in an environment similar to that of a cold seep (including temperature and salinity), but deprived of methane. Although *G. platifrons* mussel mortality was continuously observed during the cultivation period, dozens of mussels survived in the system for nearly 1 year. Using this system, mussels in different stress stages were successfully collected, including freshly collected mussels (InS) and mussels deprived of methane for 7 days (G7D), 4 weeks (G4W), 3 months (G3M) and 1 year (G1Y) (Fig. 1A). Quantitative real-time PCR (qRT-PCR), fluorescence *in situ* hybridization (FISH), and transmission electron microscope (TEM) analysis showed that both the density and overall number of symbionts decreased continuously under methane deprivation, and could no longer be detected after the third month (Fig. 1B, C, Fig. S1A). The robust decline of the symbiont population confirmed the substantial influence of methane deprivation, which compromised the stability of symbiotic associations. Accompanied by the decolonization of symbionts, it was also noticeable that the relative volume of secondary lysosomes in bacteriocytes increased drastically in the G7D and G4W groups in comparison with normal mussels (InS group) (Fig. 1C). The bacteriocytes disappeared gradually in the gill tissue after the third month, and were replaced with ciliated cells. These results revealed the drastic changes in the phenotype of symbiotic traits under methane deprivation and implied the influences of symbiont decolonization on the function and development of symbiotic cells and organs.

To address the phenotypic changes at the molecular level, this study then conducted both proteomic and metabolic analyses using gill tissue samples obtained from both the normal and decolonized mussels. Consequently, a total of 7821 host proteins were identified in the proteome, occupying 22.58% of total encoding genes in *G. platifrons* (Table S1). Principal component analysis (PCA) and Pearson correlation analysis

demonstrated good consistency among samples of the same group, verifying the repeatability and reliability of the proteomic data (Fig. S1B, C). In addition, by screening the differentially expressed proteins of each group in comparison with the InS group, it was found that the expression atlases of the decolonized groups (G7D, G4W, G3M, and G1Y groups) were distinctly different from those of normal mussels (InS group), while the G7D and G4W groups were highly similar to each other, sharing the majority of differentially expressed proteins (Fig. S1D). The distinct expression atlases demonstrated the vigorous molecular response of deep-sea mussels against methane deprivation and indicated that the hosts might adopt different strategies during the early-stage (the G7D and G4W groups), middle-stage (the G3M group), and long-term (the G1Y group) stress. In support of this speculation, functional enrichment analysis of the differentially expressed proteins also showed that the hosts employed distinct biological processes in different stage of methane deprivation, ranging from cell metabolism to cytoskeleton/organelle rearrangement and cell proliferation/differentiation (Fig. S2, Fig. S3, and Table S2). In accordance with the proteomic results, metabolomics analysis also showed distinct metabolic patterns between groups (Fig. S4, Table S3, and Table S4). The dynamic modulations of the cell metabolism, cytoskeleton/organelle rearrangement, and cell proliferation/differentiation were consistent with the morphological changes observed in the FISH and TEM assays, and provided valuable information to on the influence of symbionts during the methane deprivation process.

Lysosome-mediated digestion promoted symbiont depletion at the early stage of methane deprivation

Among the morphological changes of bacteriocytes that occurred shortly after methane deprivation, the depletion of symbionts was of great importance as the symbionts served as the major nutrition sources of their hosts. With high-resolution TEM images of bacteriocytes, methanotroph debris was observed in the lysosome, indicating the participation of lysosome-mediated digestion in the symbiont depletion (Fig. 2A). In support of this speculation, it was noted that the majority (11/13) of the differentially expressed proteins involved in the lysosome were up-regulated (Fig. 2B).

Accompanied by the enhancement of lysosome activity, several key enzymes involved in the β-oxidation of fatty acids of the peroxisome, including acyl-CoA oxidase (ACOX1), enoyl-CoA hydratase 2 (ECH2), carnitine O-palmitoyltransferase 1 (CPT1A), and (3R)-3-hydroxyacyl-CoA dehydrogenase (HSD17B4)[16], were also found to be promoted (Fig. 2C), resulting in the accumulation of some intermediates of fatty acid oxidation such as lysophosphatidylcholine, lysophosphatidylethanolamine, and carnitine (Fig. 2D). The rapid promotion of lysosome and peroxisome activity confirmed the participation of lysosome-mediated digestion in symbiont depletion, which is an essential way for the host to obtain nutrition when symbionts became infertile after being deprived of methane.

It was also noteworthy that the continuous digestion of symbionts further led to eutrophication in the gill cells, as evidenced by the robust promotion of host gluconeogenesis and glycerol synthesis--related proteins. In detail, three phosphoenolpyruvate carboxykinase (PCK) proteins, rate-limiting enzymes in gluconeogenesis[17], were dramatically up-regulated in the G7D group (Fig. 2E). Several gluconeogenesis-related carbohydrates, including glucose, glucose 6-phosphate, fructose 6-phosphate, pyruvic acid, malic acid, and citric acid, were also significantly accumulated in the metabolome of the G7D group (Fig. 2F). Similarly, aldehyde reductase (AKR1B) protein, a key enzyme involved in glycerol synthesis[18], was also found to be up-regulated in the G7D group (Fig. 2G), accompanied by newly synthesized lipid droplets in bacteriocytes (Fig. 2A). These findings suggested that the mussel host could further store extra nutrition obtained from the lysosome-mediated digestion of symbionts shortly after methane deprivation. These nutrients were crucial under prolonged methane deprivation.

Apoptosis of bacteriocytes highlighted the developmental changes of the gill after symbiont depletion

As methane deprivation and symbiont depletion continued, the morphology and population atlas of gill cells began to change noticeably. In particular, most of the bacteriocytes were replaced by ciliated cells or gill cells with microvilli, and few bacteriocytes were retained (Fig. 3A), suggesting that the mussel host adjusted the

development of gill tissue in response to prolonged methane deprivation. This study then examined the proteomics data of the G3M group to screen possible genes and processes guiding these developmental changes. Consequently, two caspase proteins (caspase 2 and caspase 7) were found to be significantly up-regulated in the G3M group in comparison with mussels during the early stage of methane deprivation (G7D group), implying the participation of cell apoptosis in the abolition of bacteriocytes (Fig. 3B). In support of this speculation, some of the remaining bacteriocytes were found to undergo apoptosis in the G3M group (Fig. 3C), with shrunken cellular size, irregular cell nuclei, condensed chromatin, and phagocyte-mediated phagocytosis[19]. In addition, diverse proteins involved in cell proliferation and differentiation, including neurofibromin 1 (NF1), epidermal growth factor receptor (EGFR), dual specificity protein phosphatase (DUSP1 and DUSP3), cytosolic phospholipase A2 (PLA2G4), sphingosine kinase (SPHK), serine/threonine-protein phosphatase 2B catalytic subunit (PPP3C), and prostaglandin-endoperoxide synthase 2 (PTGS2)[20–23], were also significantly up-regulated in the G3M group in comparison with the G7D or InS group (Fig. 3D), which possibly contributed to the proliferation of ciliated cells and collectively verified the developmental changes of gill tissue.

With the depletion of symbionts and apoptosis of bacteriocytes, the mussels could no longer obtain nutrition from symbionts. This study then sought to determine how the mussel hosts adjusted their metabolism to meet their nutritional needs. While the host down-regulated the symbiont-digestion process, it was found that proteins involved in the turnover and transition of essential metabolites, especially sterols and amino acids, were robustly promoted. For example, neutral cholesterol ester hydrolase 1 (NCEH1) protein, a key enzyme involved in hydrolyzing cholesterol ester into cholesterol[24], was significantly up-regulated in the G3M group (Fig. 3E). In addition, host genes involved in protein digestion and absorption, such as collagen and solute carrier family members (SLC3A1 and SLC7A8), as well as amino acid cycling, such as the aminoacyl-tRNA synthetases, were also significantly up-regulated[25,26] (Fig. 3E). The up-regulation of these proteins suggested that the host was promoting the

turnover process of essential metabolites to satisfy its nutritional needs in the absence of symbionts. In accordance with the proteomics result, robust increases of cholesterol, lanosterol, epicholestanol, cholecalciferol, and other sterol intermediates were observed in the G3M group, in comparison with mussels at the early stage of methane deprivation (Fig. 3F). Similarly, concentrations of some essential amino acids, such as arginine, proline, glycine, valine, ornithine, and alanine, and some proteolytic intermediates, such as Pro-Leu and Gly-Phe, were also found to be increased in the G3M group (Fig. 3G). The promotion of the turnover and transition of essential metabolites was consistent with the finding that mussel hosts stored extra nutrition obtained from the lysosome-mediated digestion of symbionts. These responses are also widely observed in other holobionts when their symbiotic associations collapse due to environmental stress.

Enhanced filter-feeding function facilitated long-term survival without symbionts

As mentioned above, the methanotrophic deep-sea mussels managed to survive for almost one year under methane deprivation. This finding raised the question of how the mussel hosts adjusted the metabolism and function of gill tissue after the abolition of bacteriocytes and replenishment of ciliated cells. Although it was speculated that the mussels could continue down-regulate their energy-consuming processes to conserve nutrition, functional enrichment analysis demonstrated robust increases in the glucose metabolism and amino acid metabolism in the gill tissue of the G1Y group. Noticeably, the comprehensive promotion of glycolysis, the TCA cycle, and oxidation phosphorylation were observed in mussels from the G1Y group, and were evidenced by the up-regulation of key enzymes, such as aldose 1-epimerase (galM), glucose-6-phosphate 1-epimerase, 6-phosphofructokinase 1 (pfkA), fructose-bisphosphate aldolase (ALDO), pyruvate carboxylase (PC), citrate synthase (CS), aconitate hydratase (ACO), 2-oxoglutarate dehydrogenase (OGDH), succinyl-CoA synthetase beta subunit LSC1/2, succinate dehydrogenase, fumarate hydratase (fumA), malate dehydrogenase (MDH1), NADH dehydrogenase, ubiquinol-cytochrome c reductase CYC/QCR7, and cytochrome c oxidase[27,28] (Fig. 4A, B). NCEH1 was found to be continuously up-regulated in the G1Y group, confirming that mussels were still

using stored nutrition via fatty acid oxidation (Fig. S4D). In addition to the up-regulation of fatty acid oxidation, proteins involved in the oxidation of amino acids were also up-regulated and confirmed by the sharp decrease of glutamine, glutamate, alanine, and ornithine in the metabolomics analysis (Fig. 4B). These amino acids could serve as supplementary sources of energy under long-term methane deprivation and symbiont depletion[27]. Four mitophagy-related enzymes, including TBC1 domain family member 15 (TBC1D15), serine/threonine-protein phosphatase (PGAM5), optineurin (OPTN) and Ras-related protein M-Ras (MRAS) were also found to be promoted in the G1Y group (Fig. 4C), promoting the homeostasis of cellular metabolism and sheltering the cell from oxidative damage[29].

Accompanied by the robust promotion of energy production, it was noted that proteins involved in cytoskeleton rearrangement and cilium movement were also robustly up-regulated in the G1Y group in comparison with the G3M group (Fig. 4D). The enhancement of cilium movement was consistent with the observation that the host replaced bacteriocytes with ciliated cells, and implied the promotion of the filter-feeding function of the gill, which could help the host obtain nutrition from surrounding environment and therefore enable the long-term survival of the host under methane deprivation[30]. In addition to the enhancement of cilium movement, signs of proliferating cells were also observed in the gill tissue of the G1Y group (Fig. 4E). While cell proliferation consumes massive energy, this process guarantees a continuous supply of new cells, including ciliated cells and probably bacteriocytes, in order to mount a rapid and dynamic response to either prolonged methane deprivation or the rejuvenation of methane seepage. In support of this speculation, a more intensive signal of cell proliferation was observed in the G1Y mussels that were returned and transplanted to the seepage region or the low-methane region of the cold seep, showing that the host altered gill development for the rejuvenation of methane (Fig. 4E). Consistent with this finding, researchers have reported the successful reestablishment of symbiotic associations in decolonized deep-sea mussels after resupplying the mussels with methane or sulfide[31], confirming the speculation in the present study that the mussels could regain bacteriocytes after losing them.

Sterol-related signaling pathway triggered the phenotypic changes of gill tissue

To further reveal the modulatory networks guiding the dynamic changes of gill tissue, weighted gene co-expression network analysis (WGCNA) was conducted using the proteome data, with a focus on hub proteins and signal transducers for each stage of methane deprivation. It was hypothesized that the proteins responsible for the phenotypic changes could share a coordinated expression pattern across samples, while the transcription factors or signal transducers with high interconnectivity could play crucial roles in modulating the phenotypic changes. Consequently, a total of 18 co-expression modules were obtained for the proteome of deep-sea mussels, while the blue, green, turquoise, purple, and brown modules were of particular interest and contained the majority of differentially expressed proteins in the G7D/G4W, G3M, and G1Y groups in comparison with the InS group (blue, green, and purple modules), the G7D group (turquoise module), or the G3M group (brown module), respectively (Fig. S5). About 42 differentially expressed proteins from the G7D/G4W group (in comparison with the InS group) were found to be highly interconnected within the blue module, and were involved in cell metabolism, signal transduction, and transcription regulation. Among these proteins, six proteins, including nuclear receptor-binding factor 2 (NRBF2) and ATP-dependent RNA helicase A (DHX9), were annotated as transcription regulators (Fig. 5A). In particular, NRBF2 protein, a crucial regulator in starvation-induced autophagy[32], showed the highest interconnectivity degree with the remaining differentially expressed proteins (connecting 33 of these proteins), which might serve as the hub regulators at the early stage of methane deprivation. In addition to the NRBF2 protein, HSD17B4 was also found to have a high interconnectivity degree with the differentially expressed proteins of the blue module (Fig. 5A), suggesting the participation of sterol and steroid hormone metabolism in regulating methane-deprivation-induced phenotypic changes[33]. In accordance with these findings, two additional sterol-related signaling pathway proteins (24-hydroxycholesterol 7 alpha-hydroxylase[34] and nuclear receptor coactivator 6[35]) were also found to be differentially expressed in the G7D group, accompanied by the drastic alterations of sterol-related metabolites in gill tissue.

These results collectively suggest that the sterol-related signaling pathway may play a crucial role in initiating the metabolic and developmental changes of gill tissue shortly after methane deprivation[36] (Fig. 5B). It was also noteworthy that the sterol metabolism of the host was highly coordinated with symbionts[37], which implied the potential influence of symbiont depletion in initiating the phenotypic changes of symbiotic cells and organs via the sterol-related signaling pathway.

Similarly, a total of 14 transcription regulators, including endothelial differentiation-related factor 1 (EDF1), chromatin target of PRMT1 protein (CHTOP), RNA polymerase-associated protein RTF1 homolog (RTF1), protein ecdysoneless homolog (ECD), zinc finger protein 260 (ZNF260), and EGFR, were identified in the green and turquoise modules, modulating cell metabolism, development, and differentiation processes during middle-stage methane deprivation (Fig. S6A). It was interesting to note that the cholesterol 24-hydroxylase (CYP46A1) protein, another gene involved in sterol turnover and the biosynthesis of steroid hormone[38], was also up-regulated in the G3M group and exhibited the highest interconnectivity with other proteins, verifying the ongoing contribution of the sterol-related signaling pathway in response to methane deprivation (Fig. 5B). Comparatively, four transcription regulators, including ELKS/Rab6-interacting/CAST family member 1 (ERC1), host cell factor 1 (HCFC1), protein split ends (SPEN), and translation regulators speckle targeted PIP5K1A-regulated poly(A) polymerase (TUT1), were found to be differentially expressed in the G1Y group, potentially influencing the expression of 59 proteins that were involved in cell metabolism and cilium movement, therefore constituting the core modulatory network under long-term methane deprivation (Fig. 5B and Fig. S6B, C).

Discussion

Symbiotic cells and organs provide mutualist services to their host via the intimate interaction with symbionts, and are implicated as key traits of symbiosis[4]. However, how these symbiotic traits evolve under and adapt to emerging environmental changes and how symbiotic associations influence the phenotypic changes of symbiotic cells and organs remain less investigated[3,39]. In this study, the phenotypic changes of gill

tissue from methanotrophic deep-sea mussels during long-term methane deprivation and symbiont depletion were thoroughly assessed based on the integrated data from proteome and metabolome analyses. The results showed that the hosts vigorously remodeled the metabolism, development, and function of gill tissue in response to methane deprivation and to sustain long-term survival without symbionts, which were guided by a set of transcription factors and sterol-related signaling pathway and influenced by the symbiont sterol metabolism. The present study has uncovered the robust phenotypic plasticity of symbiotic organs in deep-sea mussels, which facilitates the evolution and adaptation of deep-sea mussels and is crucial in understanding and protecting the biodiversity of marine fauna from the growing influence of anthropogenic activities, such as deep-sea mining.

Obtaining sufficient nutrition is the top priority for deep-sea organisms living in extreme environments with limited organic carbon. While deep-sea mussels can harvest nutrition from their chemosynthetic endosymbionts under normal conditions via either “milking” way or “farming” way [40,41], homeostasis can be compromised instantly once the surrounding reduced components are decreased and symbionts became infertile. In the present study, the metabolic processes of methanotrophic hosts were found to be robustly altered soon after methane deprivation. The deep-sea mussels sacrificed their infertile symbionts rapidly and massively to meet their nutritional needs via a lysosome-mediated digestion process. It is noteworthy that the lysosome-mediated digestion of symbionts is a common choice for almost all hosts under nutritional limitation, although this process can compromise and even destroy the symbiotic associations[41,42]. Nevertheless, symbiotic associations can recover gradually once methane or sulfide becomes available[15,31], making the sacrifice of symbionts affordable. It was also noted that the mussel host reallocated energy to sustain the proliferation of ciliated cells and enhance the filter-feeding function of the gill. These phenotypic changes were believed to benefit the harvest of environmental particulate organic matter (POM) as a supplementary way to meet the nutritional needs of the host[30]. The local environments of cold seeps and hydrothermal vents can fluctuate rapidly and vigorously due to geological activities, resulting in the aperiodic

decrease and/or increase of reduced components. Therefore, phenotypic changes in symbiotic cells and organs can occur frequently in part or in whole for deep-sea mussels regarding to the intensity of environmental change and serve as key indicators of deep-sea mining or other anthropogenic activities. Besides, the deep-sea mussel could survive even much longer than one year in natural condition since our experimental condition is much harsh[31,43]. While the phenotypic changes of the digestion system remain unexplored, the long-term survival of deep-sea mussels under methane deprivation might also endow them with transgenerational effects, allowing for a permanent transition from chemoautotrophy (a symbiotic association with thiotrophs) or chemoheterotrophy (a symbiotic association with methanotrophs) to strict heterotrophy (filter-feeding). In support of the speculation, some studies have reported the loss or reduction of symbiosis in the bathymodiolin mussel, *Idas argenteus*, which can be induced by nutrient-rich environments[12]. Collectively, these findings verify the robust plasticity of symbiotic organs in deep-sea mussels, which makes them one of the most successful holobionts in deep-sea.

While deep-sea mussels are known to harbor hundreds or thousands of symbionts inside a single bacteriocyte[44], knowledge on how symbionts influence the development of symbiotic cells and organs is still scarce. It is noteworthy that the early development of gill tissue in deep-sea mussels is quite similar to that in nonsymbiotic mussels, while the epithelial cells can become hypertrophic and lose microvilli and cilia once colonized by symbionts[45]. In addition, the newly formed bacteriocytes of adult mussels also lose microvilli after being colonized by the symbionts of adjacent bacteriocytes[13]. These morphological changes indicate that symbionts substantially influence the function and development of gill cells. In line with these findings, it was also observed that gill tissue underwent dramatic phenotypic changes during the decolonization process, suggesting that the loss of symbionts could reshape the function and development of symbiotic cells and organs. While the formation and maintenance processes of symbiotic cells are similar across different species and phyla[46,47], the characterization of the host signaling pathways and symbiont-deprived signal transducers that regulate the process remains

challenging[48–50]. Here, the findings suggested that the sterol-related signaling pathway could play important roles in reshaping the metabolism, function, and development of gill tissue once the symbionts were depleted. Moreover, the differential expression of the sterol-related signaling pathway under methane deprivation might be a cascade reaction triggered by the shortage of symbiont-deprived sterol intermediates[37]. In support of this speculation, data from the single-cell transcriptome analysis also suggested that the methanotrophic symbionts could influence the differentiation and maturation processes of bacteriocytes via the sterol-related signaling pathway[43]. It is also noticeable that majority of animal hosts have formed coordinated sterol metabolism with their symbionts, highlighting the possible role of sterol-related signaling pathway in the phenotypic plasticity of symbiotic cells and organs across different holobionts.

In summary, this study comprehensively depicted the robust phenotypic plasticity of gill tissue in response to methane deprivation and symbiont depletion based on the integrated multi-omics data. In addition, the dynamic remodeling of the cell metabolism, development, and function of gill tissue facilitated the long-term survival of deep-sea mussels even the loss of all symbionts, which could support the range and persistence of mussels in the extreme environment of the deep sea and help the mussels to adapt to and evolve in emerging environmental changes. The robust phenotypic plasticity of gill tissue also implied the outstanding resilience ability the deep-sea mussel community, making deep-sea mussels promising models in evaluating the ecological influences of deep-sea mining. However, there were still some limitations in the current study. For example, the long-term methane deprivation assay was conducted *ex situ* instead of *in situ*, which could have caused disturbance to the deep-sea mussels[51]. In addition, the exact mechanism and target cells of the sterol-related signaling pathway need to be further verified *in vivo* in future studies to fully understand the phenotypic plasticity of gill tissue. While these limitations remain a common challenge for studies on deep-sea organisms, the present study has nevertheless shed new light on understanding the symbiotic interaction and environmental adaptation of deep-sea mollusks.

Materials and methods

Mussel collection and methane-deprivation assay

G. platifrons mussels were collected from a cold seep (22°06′N, 119°17′E) in the South China Sea using the "Faxian," a remotely operated vehicle, during a research cruise in 2017. The mussels were transferred to the deck for less than 1 h using an isobaric and/or isothermal biobox that could shelter them from depressurization and elevated temperature during recovery[51]. Once aboard, the gill tissues from six mussels were collected to indicate the *in situ* state (the InS group, containing isobaric and isothermal samples). The remaining mussels (isothermal samples) were transferred to the onboard recirculating system (atmospheric pressure) for acclimation. To mimic the *in situ* environment, the system was supplied with surface seawater from the cold seep and kept at 3.5 ± 0.5°C and 34.5 ± 0.5‰ salinity, with half of the water replaced every day. After the cruise, the mussels were transferred into a recirculating system inside the laboratory with same environmental parameters[52], although the particulate organic carbon concentration was elevated from 1.6–4 μM to 20–60 μM[53–55]. To completely deplete the symbiotic methanotrophs, a final concentration of 50 mg/L ampicillin and kanamycin was added to the seawater for the first month after recovery, while no methane was added to the recirculating system during the whole assay. At days 7, 28, 84, and 288 post mussel recovery, six mussels were randomly collected to represent different stress stages (designated as the G7D, G4W, G3M, and G1Y groups, respectively). For all sampled mussels, a portion of the gill filaments was fixed with 4% paraformaldehyde or a mixture of paraformaldehyde and glutaraldehyde (2%/2.5%) for the subsequent FISH and TEM assays. The remaining gills were frozen with liquid nitrogen and stored at −80°C for symbiont quantification, proteome analysis (only gills from three mussels were used), and metabolome analysis (the G4W group was excluded from the analysis). At day 309 after mussel recovery, another 18 live mussels were injected with 5-ethynyl 2′-deoxyuridine (EdU, 5×10^{-9} mol/individual) in the adductor muscle to label the newly generated gill cells. Among the injected mussels, six were continuously cultured in the recirculating system, while the

remaining mussels were returned to the seepage region or a low-methane region of the cold seep using the isothermal biobox. The EdU-treated mussels were collected 5 days later for gill tissue sampling and fixed with paraformaldehyde or paraformaldehyde/glutaraldehyde for EdU staining and TEM analysis.

Proteome analysis

Proteome analysis was conducted with assistance by PTM Biolabs (Hangzhou, China). The proteome analysis methods are described in detail in the supplementary material. In brief, gill proteins were extracted and digested by trypsin. The peptides obtained by trypsin digestion were subsequently labeled as directed by the tandem mass tag (TMT) kit (PTM Biolabs). The labeling peptides were then fractionated by high pH reverse-phase high-performance liquid chromatography and further subjected to liquid chromatography with tandem mass spectrometry (LC-MS/MS) analysis. LC-MS/MS spectra were searched against the *G. platifrons* genome data concatenated with the reverse decoy database.

Gene Ontology (GO) and KEGG annotations of the *G. platifrons* proteome were derived from the integrated analysis by non-redundant protein sequences of the NCBI, the KEGG database, UniProt, Pfam, and InterProScan.

Metabolome analysis

The detailed metabolome analysis methods are described in the supplementary material. In brief, gill tissues were treated with 80% methanol to release all metabolites. After centrifugation at 12,000 g and 10°C for 15 min, the supernatants were divided into four parts and subjected to liquid chromatography–mass spectrometry (LC-MS), gas chromatography/mass spectrometry (GC–MS), and the corresponding quality control analysis.

The raw spectra obtained by LC-MS and GC-MS were decoded by MetaboAnalyst (https://www.metaboanalyst.ca/MetaboAnalyst/ModuleView.xhtml), and all identified metabolites were annotated with Human Metabolome Database (HMDB), PubChem, and the KEGG database. For the identification of differential metabolites, a PCA analysis was first conducted to validate the consistency of parallel samples within the same group and exclude outlier samples. Then, the differentially abundant metabolites

were screened by both OPLS-DA and the Wilcoxon rank sum test.

WGCNA

WGCNA is conducted to identify proteins with correlated expression patterns in all groups. Co-expression networks were constructed using the WGCNA package (v1.47) in the R software after incorporating the protein abundance (power = 6). The correlation coefficients of samples were then calculated based on the module eigengenes. The intramodular connectivity and module correlation degree of each gene was also calculated by the R package of WGCNA to determine the hub genes. Finally, the networks were visualized using Cytoscape (v3.8.2).

Symbiont quantification, TEM imaging, FISH, and EdU staining

Changes in symbiont abundance during the methane deprivation assay were monitored by quantitative real-time PCR (qRT-PCR) using previously described methods[56]. Briefly, the methane monooxygenase subunit A gene (*pmoA*), a marker gene in methanotrophic symbionts, was used to indicate the symbiont abundance, while the mussel actin gene was used as an internal control. The genomic DNA of gill tissues was extracted using a mollusk DNA extraction kit (Omega Bio-tek, Norcross, GA, USA) for the template. The primers and qRT-PCR programs used were the same as described in previous reports.

TEM of the gills was conducted following the method described in a previous study[57]. In brief, gill samples fixed by paraformaldehyde-glutaraldehyde were treated with 1.0% osmium tetroxide (OsO_4) for staining and then dehydrated with alcohol. After infiltration with acrylic resin, the samples were finally embedded and sectioned with a thickness of 70 nm using an ultramicrotome (EM UC7, Leica, Vienna, Austria). After staining by uranyl acetate and lead citrate, the gill cell ultrastructure was imaged with a transmission electron microscope (HT7700, Hitachi, Tokyo, Japan).

The FISH assay of symbionts was conducted using gill filament samples from the InS, G7D, G3M, and G1Y groups according to the method described by Halary et al. (53). In brief, gill samples fixed by paraformaldehyde were first dehydrated and embedded in paraffin. After they were cross-sectioned to 7 μm in thickness, the gill tissues were incubated with a Cy3-labeled methanotroph-specific probe (*pmoB* gene,

5’CGAGATATTATCCTCGCCTG3’) for hybridization. After staining the nucleic acids with 4′, 6-diamidino-2-phenylindole (DAPI), gill sections were imaged with a fluorescence microscope (Nikon ECLIPSE Ni, Tokyo, Japan) to demonstrate the spatial distribution of symbiotic methanotrophs.

EdU staining was also conducted with the paraffin sections. In brief, after treatment with 4% paraformaldehyde and dehydration with ethanol, EdU-labeled gills were embedded in paraffin and sectioned using a microtome (Leica, Heidelberg, Germany) to a thickness of 7 μm. The EdU staining was conducted using the Click-iT Plus EdU Imaging Kit (Thermo Fisher, Waltham, MA, USA) and visualized with a fluorescence microscope (Nikon ECLIPSE Ni, Tokyo, Japan) after deparaffinization and rehydration.

Statistical analyses

For the identification of differentially expressed proteins, the expression values across all samples were first quantified and the mean values of each group were used for subsequent comparison. Proteins were considered to be differentially expressed only when the fold changes between two given groups were greater than 1.2-fold, with a p value less than 0.05 (two-tailed *t*-test). For the GO enrichment analysis, the differentially expressed proteins were classified into three categories (biological process, cellular component, and molecular function) and subjected to two-tailed Fisher’s exact test (adjusted p-value < 0.05) to determine the significance against all identified proteins. For KEGG enrichment analysis, the two-tailed Fisher’s exact test was also used, and the results were further mapped to the pathways using the online KEGG mapper service tool. For the qRT-PCR assay, six biological replicates were employed for each group, and the relative abundance was calculated using the $2^{-\Delta\Delta Ct}$ method and given as the mean ± s.d. A Kruskal–Wallis test followed by Dunn’s multiple comparison was employed to determine the significant differences between groups.

Acknowledgments

We thank the crew members of the R/V Kexue for their assistance in sample collection and the laboratory staff for continuous technical advice and helpful discussions. We also thank Professor Guowang Xu and Professor Xinjie Zhao for their assistance in the metabolome analysis. We also thank Prof. Qiang Lin from the South China Sea Institute of Oceanology, Chinese Academy of Sciences for insightful comments and suggestions that improved the manuscript.

Funding: The present study was supported by the National Natural Science Foundation of China (42030407, 42106134, and 42076091), the Key Research Program of Frontier Sciences (ZDBS-LY-DQC032), the Marine S&T Fund of Shandong Province for the Pilot National Laboratory for Marine Science and Technology (Qingdao) (No. 2022QNLM030004), the Strategic Priority Research Program of the Chinese Academy of Sciences (XDA22050303 and XDB42020401), and the Key Deployment Project of the Center for Ocean Mega-Science, CAS (COMS2020Q02).

Author contributions: M.L. and H.C. participated in the study design and data interpretation. H.C., M.W., S. Z., and C. Lian helped in the sample collection. M.L. conducted the majority of the experimental work and data analysis and drafted the manuscript. Y.L., M.W., S. Z., L.Z., H.Z., and H.W. assisted with the interpretation of the results. L.C. surveyed environmental parameters during the cruise. H.C. and C. Li conceived the study, coordinated the experiments, and helped draft the manuscript. All authors gave their final approval for publication.

Competing interests: The authors declare no competing interests.

Data accessibility: All data needed to evaluate the conclusions in the paper are presented in the paper and/or the supplementary materials. All proteomic raw data have been deposited into the iProX Consortium (https://iprox.org/) with the project ID IPX0004524000.

Reference

1 Agrawal Anurag, A. Phenotypic plasticity in the interactions and evolution of species. *Science* **294**, 321-326, doi:10.1126/science.1060701 (2001).

2 Moran, N. A. Symbiosis as an adaptive process and source of phenotypic complexity. *Proceedings of the National Academy of Sciences* **104**, 8627-8633, doi:10.1073/pnas.0611659104 (2007).

3 Gilbert, S. F., Bosch, T. C. G. & Ledón-Rettig, C. Eco-Evo-Devo: developmental symbiosis and developmental plasticity as evolutionary agents. *Nature Reviews Genetics* **16**, 611-622, doi:10.1038/nrg3982 (2015).

4 Douglas, A. E. Housing microbial symbionts: evolutionary origins and diversification of symbiotic organs in animals. *Philosophical Transactions of the Royal Society B: Biological Sciences* **375**, 20190603, doi:10.1098/rstb.2019.0603 (2020).

5 McFall-Ngai Margaret, J. & Ruby Edward, G. Symbiont recognition and subsequent morphogenesis as early events in an animal-bacterial mutualism. *Science* **254**, 1491-1494, doi:10.1126/science.1962208 (1991).

6 Braendle, C. *et al*. Developmental origin and evolution of bacteriocytes in the aphid–Buchnera symbiosis. *PLoS Biology* **1**, e21, doi:10.1371/journal.pbio.0000021 (2003).

7 Matsuura, Y., Kikuchi, Y., Miura, T. & Fukatsu, T. Ultrabithorax is essential for bacteriocyte development. *Proceedings of the National Academy of Sciences* **112**, 9376-9381, doi:10.1073/pnas.1503371112 (2015).

8 Dubilier, N., Bergin, C. & Lott, C. Symbiotic diversity in marine animals: the art of harnessing chemosynthesis. *Nature Reviews Microbiology* **6**, 725, doi:10.1038/nrmicro1992 (2008).

9 Duperron, S. *et al.* An overview of chemosynthetic symbioses in bivalves from the North Atlantic and Mediterranean Sea. *Biogeosciences* **10**, 3241-3267, doi:10.5194/bg-10-3241-2013 (2013).

10 Sun, J. *et al.* Adaptation to deep-sea chemosynthetic environments as revealed by mussel genomes. *Nature Ecology & Evolution* **1**, 121, doi:10.1038/s41559-017-0121 (2017).

11 Lorion, J. *et al*. Adaptive radiation of chemosymbiotic deep-sea mussels. *Proceedings of the Royal Society B: Biological Sciences* **280**, 20131243,

doi:10.1098/rspb.2013.1243 (2013).

12 Rodrigues, C. F. *et al*. A sad tale: has the small mussel *Idas argenteus* lost its symbionts. *Biological Journal of the Linnean Society* **114**, 389-405, doi:10.1111/bij.12431 (2015).

13 Wentrup, C., Wendeberg, A., Schimak, M., Borowski, C. & Dubilier, N. Forever competent: deep-sea bivalves are colonized by their chemosynthetic symbionts throughout their lifetime. *Environmental Microbiology* **16**, 3699-3713, doi:10.1111/1462-2920.12597 (2014).

14 Sibuet, M. & Olu, K. Biogeography, biodiversity and fluid dependence of deep-sea cold-seep communities at active and passive margins. *Deep Sea Research Part II: Topical Studies in Oceanography* **45**, 517-567, doi: 10.1016/S0967-0645(97)00074-X (1998).

15 Kádár, E. *et al*. Experimentally induced endosymbiont loss and re-acquirement in the hydrothermal vent bivalve *Bathymodiolus azoricus*. *Journal of Experimental Marine Biology and Ecology* **318**, 99-110, doi:10.1016/j.jembe.2004.12.025 (2005).

16 Poirier, Y., Antonenkov, V. D., Glumoff, T. & Hiltunen, J. K. Peroxisomal β-oxidation—A metabolic pathway with multiple functions. *Biochimica et Biophysica Acta (BBA) - Molecular Cell Research* **1763**, 1413-1426, doi: 10.1016/j.bbamcr.2006.08.034 (2006).

17 Yu, S., Meng, S., Xiang, M. & Ma, H. Phosphoenolpyruvate carboxykinase in cell metabolism: Roles and mechanisms beyond gluconeogenesis. *Molecular Metabolism* **53**, 101257, doi:10.1016/j.molmet.2021.101257 (2021).

18 Hagopian, K., Ramsey, J. J. & Weindruch, R. Enzymes of glycerol and glyceraldehyde metabolism in mouse liver: effects of caloric restriction and age on activities. *Bioscience Reports* **28**, 107-115, doi:10.1042/BSR20080015 (2008).

19 Bonanno, E. *et al*. Cell shape and organelle modification in apoptotic U937 cells. *European Journal of Histochemistry : EJH* **44**, 237-246 (2000).

20 Wee, P. & Wang, Z. Epidermal growth factor receptor cell proliferation signaling pathways. *Cancers* **9**, 52, doi: 10.3390/cancers9050052 (2017).

21 Kohno, M. *et al.* Intracellular role for sphingosine kinase 1 in intestinal adenoma

cell proliferation. *Molecular and Cellular Biology* **26**, 7211-7223, doi: 10.1128/MCB.02341-05 (2006).

22 Dasgupta, B. & Gutmann, D. H. Neurofibromin regulates neural stem cell proliferation, survival, and astroglial differentiation *in vitro* and *in vivo*. *The Journal of Neuroscience* **25**, 5584, doi:10.1523/JNEUROSCI.4693-04.2005 (2005).

23 Hooks, S. B. & Cummings, B. S. Role of Ca^{2+}-independent phospholipase A2 in cell growth and signaling. *Biochemical Pharmacology* **76**, 1059-1067, doi:10.1016/j.bcp.2008.07.044 (2008).

24 Zhang, S., Glukhova, S. A., Caldwell, K. A. & Caldwell, G. A. NCEH-1 modulates cholesterol metabolism and protects against α-synuclein toxicity in a C. elegans model of Parkinson's disease. *Human Molecular Genetics* **26**, 3823-3836, doi:10.1093/hmg/ddx269 (2017).

25 Cusack, S. Aminoacyl-tRNA synthetases. *Current Opinion in Structural Biology* **7**, 881-889, doi:10.1016/S0959-440X(97)80161-3 (1997).

26 Fotiadis, D., Kanai, Y. & Palacín, M. The SLC3 and SLC7 families of amino acid transporters. *Molecular Aspects of Medicine* **34**, 139-158, doi:10.1016/j.mam.2012.10.007 (2013).

27 Akram, M. Citric acid cycle and role of its intermediates in metabolism. *Cell Biochemistry and Biophysics* **68**, 475-478, doi:10.1007/s12013-013-9750-1 (2014).

28 Chandel, N. S. Glycolysis. *Cold Spring Harbor Perspectives in Biology* **13**, doi:10.1101/cshperspect.a040535 (2021).

29 Dengjel, J. & Abeliovich, H. Roles of mitophagy in cellular physiology and development. *Cell and Tissue Research* **367**, 95-109, doi:10.1007/s00441-016-2472-0 (2017).

30 Page, H. M., Fisher, C. R. & Childress, J. J. Role of filter-feeding in the nutritional biology of a deep-sea mussel with methanotrophic symbionts. *Marine Biology* **104**, 251-257, doi:10.1007/BF01313266 (1990).

31 Hiebenthal, C., Gehlert, F.-O., Schmidt, M., Reusch, T. B. H. & Melzner, F. Long-term culture system for deep-sea mussels *Gigantidas childressi*. Preprint at *https://www.biorxiv.org/content/10.1101/2021.11.24.469854v1* (2021).

32 Ma, X. *et al*. MTORC1-mediated NRBF2 phosphorylation functions as a switch for the class III PtdIns3K and autophagy. *Autophagy* **13**, 592-607, doi:10.1080/15548627.2016.1269988 (2017).

33 Griffiths, W. J. *et al*. Additional pathways of sterol metabolism: Evidence from analysis of Cyp27a1$^{-/-}$ mouse brain and plasma. *Biochimica et Biophysica Acta (BBA) - Molecular and Cell Biology of Lipids* **1864**, 191-211, doi:10.1016/j.bbalip.2018.11.006 (2019).

34 Chiang, J. Y. L. & Ferrell, J. M. Up to date on cholesterol 7 alpha-hydroxylase (CYP7A1) in bile acid synthesis. *Liver Research* **4**, 47-63, doi:10.1016/j.livres.2020.05.001 (2020).

35 McKenna, N. J. & O'Malley, B. W. Minireview: nuclear receptor coactivators—an update. *Endocrinology* **143**, 2461-2465, doi:10.1210/endo.143.7.8892 (2002).

36 Wollam, J. & Antebi, A. Sterol regulation of metabolism, homeostasis, and development. *Annual Review of Biochemistry* **80**, 885-916, doi:10.1146/annurev-biochem-081308-165917 (2011).

37 Takishita, K. *et al.* Genomic evidence that methanotrophic endosymbionts likely provide deep-sea bathymodiolus mussels with a sterol intermediate in cholesterol biosynthesis. *Genome Biology and Evolution* **9**, 1148-1160, doi:10.1093/gbe/evx082 (2017).

38 Russell, D. W., Halford, R. W., Ramirez, D. M., Shah, R. & Kotti, T. Cholesterol 24-hydroxylase: an enzyme of cholesterol turnover in the brain. *Annual Review of Biochemistry* **78**, 1017-1040, doi:10.1146/annurev.biochem.78.072407.103859 (2009).

39 Bénard, A., Vavre, F. & Kremer, N. Stress & symbiosis: heads or tails? *Frontiers in Ecology and Evolution* **8**, doi: 10.3389/fevo.2020.00167 (2020).

40 Kádár, E., Davis, S. A. & Lobo-da-Cunha, A. Cytoenzymatic investigation of intracellular digestion in the symbiont-bearing hydrothermal bivalve *Bathymodiolus azoricus*. *Marine Biology* **153**, 995-1004, doi:10.1007/s00227-007-0872-0 (2008).

41 Sogin, E. M., Leisch, N. & Dubilier, N. Chemosynthetic symbioses. *Current Biology* **30**, R1137-R1142, doi:10.1016/j.cub.2020.07.050 (2020).

42 Bright, M., Keckeis, H. & Fisher, C. R. An autoradiographic examination of

carbon fixation, transfer and utilization in the *Riftia pachyptila* symbiosis. *Marine Biology* **136**, 621-632, doi:10.1007/s002270050722 (2000).

43 Chen, H. *et al*. Single-cell perspectives on the function and development of deep-sea mussel bacteriocytes. Preprint at https://www.biorxiv.org/content/10.1101/2022.05.28.493830v1 (2022).

44 Halary, S., Riou, V., Gaill, F., Boudier, T. & Duperron, S. 3D FISH for the quantification of methane- and sulphur-oxidizing endosymbionts in bacteriocytes of the hydrothermal vent mussel *Bathymodiolus azoricus*. *The ISME journal* **2**, 284-292, doi:10.1038/ismej.2008.3 (2008).

45 Franke, M., Geier, B., Hammel, J. U., Dubilier, N. & Leisch, N. Coming together—symbiont acquisition and early development in deep-sea bathymodioline mussels. *Proceedings of the Royal Society B: Biological Sciences* **288**, 20211044, doi:10.1098/rspb.2021.1044 (2021).

46 McFall-Ngai, M. J. The importance of microbes in animal development: lessons from the squid-vibrio symbiosis. *Annual Review of Microbiology* **68**, 177-194, doi:10.1146/annurev-micro-091313-103654 (2014).

47 Cossart, P. & Sansonetti, P. J. Bacterial invasion: the paradigms of enteroinvasive pathogens. *Science* **304**, 242-248, doi:10.1126/science.1090124 (2004).

48 Coon, K. L. *et al*. Bacteria-mediated hypoxia functions as a signal for mosquito development. *Proceedings of the National Academy of Sciences of the United States of America* **114**, E5362-e5369, doi:10.1073/pnas.1702983114 (2017).

49 Nyholm, S. V. & McFall-Ngai, M. J. A lasting symbiosis: how the Hawaiian bobtail squid finds and keeps its bioluminescent bacterial partner. *Nature Reviews Microbiology* **19**, 666-679, doi:10.1038/s41579-021-00567-y (2021).

50 Heath-Heckman, E. A., Foster, J., Apicella, M. A., Goldman, W. E. & McFall-Ngai, M. Environmental cues and symbiont microbe-associated molecular patterns function in concert to drive the daily remodelling of the crypt-cell brush border of the *Euprymna scolopes* light organ. *Cellular Microbiology* **18**, 1642-1652, doi:10.1111/cmi.12602 (2016).

51 Chen, H. *et al*. A glimpse of deep-sea adaptation in chemosynthetic holobionts:

depressurization causes DNA fragmentation and cell death of methanotrophic endosymbionts rather than their deep-sea Bathymodiolinae host. *Molecular Ecology*, doi:10.1111/mec.15904 (2021).

52 Cao, L. *et al. In situ* detection of the fine scale heterogeneity of active cold seep environment of the Formosa Ridge, the South China Sea. *Journal of Marine Systems* **218**, 103530, doi:10.1016/j.jmarsys.2021.103530 (2021).

53 Zhou, B. *et al.* Source, transformation and degradation of particulate organic matter and its connection to microbial processes in Jiaozhou Bay, North China. *Estuarine, Coastal and Shelf Science* **260**, 107501, doi:10.1016/j.ecss.2021.107501 (2021).

54 Yuan, H. *et al.* Spatial and seasonal variations, partitioning and fluxes of dissolved and particulate nutrients in Jiaozhou Bay. *Continental Shelf Research* **171**, 140-149, doi:10.1016/j.csr.2018.11.004 (2018).

55 Hung, J. J., Wang, S. M. & Chen, Y. L. Biogeochemical controls on distributions and fluxes of dissolved and particulate organic carbon in the Northern South China Sea. *Deep Sea Research Part II: Topical Studies in Oceanography* **54**, 1486-1503, doi:10.1016/j.dsr2.2007.05.006 (2007).

56 Sun, Y. *et al.* Molecular identification of methane monooxygenase and quantitative analysis of methanotrophic endosymbionts under laboratory maintenance in *Bathymodiolus platifrons* from the South China Sea. *PeerJ* **5**, e3565, doi:10.7717/peerj.3565 (2017).

57 Wang, H. *et al.* Molecular analyses of the gill symbiosis of the bathymodiolin mussel *Gigantidas platifrons*. *iScience* **24**, 101894, doi:10.1016/j.isci.2020.101894 (2021).

Figure 1. Phenotypic changes of gill tissue under methane deprivation.

(A) A schematic drawing of the experimental workflow. The deep-sea mussels were subjected to a long-term methane deprivation assay in a laboratory recirculating system and sampled at days 0, 7, 28, 84, and 288 (the InS, G7D, G4W, G3M, and

G1Y groups, respectively) for proteome and metabolome analyses. Mussels from the G1Y group were also subjected to a 5-ethynyl 2′-deoxyuridine (EdU)-labeling assay under laboratory conditions or after being transplanted back to the cold seep.

(B) Fluorescence *in situ* hybridization (FISH) assay of mussel gills. The Cy3-labelled symbiont-specific probe (designed based on the *pmoB* gene) was employed to indicate endosymbiotic methanotrophs (in red), while nuclei were stained using 4′, 6-diamidino-2-phenylindole (DAPI, in blue). The results showed that symbionts were depleted rapidly under the methane deprivation assay.

(C) Transmission electron microscope (TEM) analysis of cross-sectioned gill tissues. TEM images revealed the robust morphological changes of gills under methane deprivation, including depletion of symbionts and bacteriocytes and replenishment of ciliated cells.

Figure 2. Metabolic remodeling of gill tissue at the early stage of methane deprivation.

(A) Magnified transmission electron microscope (TEM) image of bacteriocytes in the InS (A_1) and G7D (A_2) groups. Methanotrophic endosymbionts were found to be greatly reduced under methane deprivation, while some digested debris was observed in the augmented lysosomes (A_3). Large volumes of lipid droplets were also observed in the bacteriocytes shortly after methane deprivation (A_4).

(B) Heatmap of differentially expressed proteins involved in lysosome-mediated digestion in the G7D group in comparison with the InS group. Up-regulated proteins are labeled in red, while down-regulated proteins are labeled in blue.

(C) Heatmap of differentially expressed proteins that involved in fatty acid metabolism in the G7D group in comparison with the InS group.

(D) Alterations in the relative abundances of lysophosphatidylcholine (LPC), lysophosphatidylethanolamine (LPE), and carnitine in the InS and G7D groups as detected by liquid chromatography–mass spectrometry (LC-MS) (data given as mean ± SD).

(E) Expression patterns of three phosphoenolpyruvate carboxykinases (PCKs)

homologous in the G7D and InS groups as revealed by the proteome (data given as the mean ± SD).

(F) Fold changes of the relative abundances of carbohydrates in the G7D group compared to the InS group as detected by gas chromatography–mass spectrometry (GC-MS).

(G) Expression pattern of aldehyde reductase (AKR1B) protein in the G7D group in comparison with the InS group.

Figure 3. Developmental and metabolic changes of gill tissue at the middle stage of methane deprivation.

(A) Transmission electron microscope (TEM) images of gill tissue in the G3M group. Few bacteriocytes were retained while most were replaced by ciliated cells at this stage.

(B) Expression patterns of two caspases (caspase2 and caspase 7) in the G3M and G7D groups as revealed by the proteome (data given as the mean ± SD).

(C) TEM imaging revealed the apoptosis of bacteriocytes with distinct morphological features, including cell shrinkage (C_1), irregular morphology of the nucleus (C_2), condensed crescent-shaped chromatin (C_3), and phagocyte-mediated phagocytosis (C_4).

(D) Heatmap of differentially expressed proteins involved in cell proliferation and differentiation in the InS group and the G3M group.

(E) Heatmap of differentially expressed proteins involved in the oxidation of lipids and amino acids in the G3M group compared to the InS group.

(F) Fold changes of the relative content of steroid metabolites in the G3M group compared to the InS group as identified by the gas chromatography–mass spectrometry (GC-MS) metabolome.

(G) Fold changes of the relative abundance of amino acids in the G3M group compared to the InS group as revealed by the liquid chromatography–mass spectrometry (LC-MS) metabolome.

Figure 4. Phenotypic changes of gill tissue under long-term methane deprivation.

(A) Fold changes of the differentially expressed enzymes involved in glycolysis, tricarboxylic acid (TCA) cycle, and oxidation phosphorylation in the G1Y group compared to the InS group.

(B) Overview of glycolysis, the TCA cycle, and amino acid metabolism under the methane deprivation assay. Metabolites identified in the metabolome are shown in bold font. Changes in the relative abundances of metabolites and proteins are illustrated in the heatmap. Columns in the heatmap (from left to right) represent the relative abundances in the InS, G7D, G3M, and G1Y groups. Asterisks represent the significant differences in the G1Y group in comparison with the InS group. Triangles represent the significant differences in the G1Y group in comparison with the G3M group.

(C) Box plot showing the four up-regulated enzymes involved in mitophagy in the G3M group compared to the InS group.

(D) Gene Ontology (GO) enrichment analysis of differentially expressed proteins in G1Y group compared to the G3M group. The top eight most significant GO terms involved in the biological process, cellular component, and molecular function are shown.

(E) 5-ethynyl 2′-deoxyuridine (EdU)-labeling assay of gill tissue under long-term methane deprivation. Mussels in the G1Y group were subjected to EdU treatment to label newly generated cells under either *ex situ* (in laboratory recirculating system) or *in situ* conditions (transplanted back to the cold seep). Newly synthesized DNA was incorporated with EdU and visualized in green fluorescence. Cell nuclei were stained by DAPI (in blue).

Figure 5. Regulatory networks of deep-sea mussels under methane deprivation.

(A) Regulatory networks of gill tissue under methane deprivation constructed using weighted gene co-expression network analysis (WGCNA). About 42 differentially expressed proteins in the G7D/G4W groups in comparison with the InS group were found to be interconnected in the blue module (A_1), constructing the hub regulatory

networks at the early stage of methane deprivation. Similarly, a total of 22 differentially expressed proteins in the G3M group in comparison with the InS group were interconnected in the green module (A_2), constructing the hub regulatory networks at the middle stage of methane deprivation.

(B) Schematic map showing the phenotypic changes at early-stage (B_1), middle-stage (B_2), and long-term (B_3) methane deprivation. Purple boxes indicate transcription regulators. Yellow boxes indicate enzymes. Blue boxes indicate metabolic processes. Solid lines or arrows show the reactions catalyzed by differentially expressed proteins identified by the proteome. Dotted lines or arrows show the reactions catalyzed by non-significantly differentially expressed proteins identified by the proteome.

Abbreviations: NRBF2: nuclear receptor binding factor 2; HSD17B4: (3R)-3-hydroxyacyl-CoA dehydrogenase; CYP39A1: 24-hydroxycholesterol 7alpha-hydroxylase; NCOA6: nuclear receptor coactivator 6; TCA: tricarboxylic acid cycle, ATP: adenosine triphosphate; CE: cholesterol ester; TG: triglyceride; PC: phosphatidylcholine; PE: phosphatidylethanolamine; SLC family: solute carrier family; NCEH1: neutral cholesterol ester hydrolase 1; CYP46A1: cholesterol 24-hydroxylase; NR1F4: nuclear receptor subfamily 1 group F member 4; NR1IN: nuclear receptor subfamily 1 group I; COL6A: collagen type VI alpha; ARS: aminoacyl-tRNA synthetase; EDF1: endothelial differentiation-related factor 1; CHTOP: chromatin target of PRMT1 protein; RTF1: RNA polymerase-associated protein RTF1 homolog; ECD: protein ecdysoneless homolog; ZNF260: zinc finger protein 260; EGFR: epidermal growth factor receptor; VEGF: vascular endothelial growth factor signaling pathway; MAPK: mitogen-activated protein kinase signaling pathway; pfkA: 6-phosphofructokinase 1; ALDO: fructose-bisphosphate aldolase; ENO: enolase; pdhB: pyruvate dehydrogenase E1 component beta subunit; MDH1: malate dehydrogenase; fumA: fumarate hydratase; SDHA/SDHB: succinate dehydrogenase (ubiquinone); LSC1/2: succinyl-CoA synthetase beta subunit; OGDH: 2-oxoglutarate dehydrogenase; IDH: isocitrate dehydrogenase; ACO: aconitate hydratase; CS: citrate synthase; GOT1: aspartate aminotransferase; ALT: alanine transaminase; PC: pyruvate carboxylase; OAT: ornithine--oxo-acid transaminase;

PCD: 1-pyrroline-5-carboxylate dehydrogenase; GGT_5: gamma-glutamyltranspeptidase; GPT: glutathione S-transferase; GLUD1_2: glutamate dehydrogenase; NADH: nicotinamide adenine dinucleotide, reduced; NAD^+: nicotinamide adenine dinucleotide, oxidized; $FADH_2$: flavin adenosine dinucleotide, reduced; FAD: flavin adenosine dinucleotide, oxidized; TBC1D15: TBC1 domain family member 15; LC3: GABA (A) receptor-associated protein; OPTN: optineurin; ERC1: ELKS/Rab6-interacting/CAST family member 1; HCFC1: host cell factor 1; SPEN: protein split ends; TUT1: translation regulators speckle targeted PIP5K1A-regulated poly(A) polymerase.

Fig. S1. Overview of gill proteome under methane deprivation.

(A) The relative abundance of the *pmoA* gene in the InS, G7D, G3M, and G1Y groups.

(B) Principal component analysis (PCA) of proteome data in all groups.

(C) Pearson correlation analysis of the proteome in all groups (red indicates high correlation, white indicates low correlation).

(D) Venn diagram of differentially expressed proteins in the G7D and G4W groups compared to the InS group.

Fig. S2. Kyoto Encyclopedia of Genes and Genomes (KEGG) enrichment analysis of differentially expressed proteins.

The significantly enriched KEGG pathways of up-regulated and down-regulated differentially expressed proteins in the G7D group (A), G4W group (B), G3M group (C), and G1Y group (D) compared to the InS group are illustrated.

Fig. S3. Gene Ontology (GO) enrichment analysis of differentially expressed proteins in the G7D, G4W, G3M, and G1Y groups compared to the InS group.

The top 20 most significant GO terms of the differentially expressed proteins of the G7D group (A), G4W group (B), G3M group (C), and G1Y group (D) compared to the InS group are illustrated. The circles from outer to inner indicate the classification of GO terms (yellow indicates biological process, blue indicates molecular function,

and green indicates cellular component), the number of background proteins in each classification (longer indicates more proteins), colored is used to indicate the *p*-value (red indicates greater significance), the numbers of up-regulated (intense purple) and down-regulated proteins (light purple), and the rich factor value of each classification (each compartment represents 0.1).

Fig. S4. Overview of metabolome analysis in the InS, G7D, G3M, and G1Y groups.

(A) Principal component analysis (PCA)of metabolites identified in the InS, G7D, G3M, and G1Y groups by liquid chromatography–mass spectrometry (LC-MS).

(B) PCA analysis of metabolites identified in the InS, G7D, G3M, and G1Y groups by gas chromatography–mass spectrometry (GC-MS).

(C) UpSet diagram of the differentially expressed proteins in the G7D, G3M, and G1Y groups compared to the InS group. The horizontal bars show the total number of differentially abundant metabolites in each methane deprivation treatment group compared to the InS group. The vertical bars show the shared number of differentially abundant metabolites between the given groups. Connected dots refer to the groups involved in each intersection.

(D) Expression pattern of neutral cholesterol ester hydrolase 1 (NCEH1) during methane deprivation (data given as the mean ± SD).

Fig. S5. Venn diagrams of differentially expressed proteins identified in the G7D, G4W, G3M, and G1Y groups and by weighted gene co-expression network analysis (WGCNA) analysis.

(A) Venn diagram of differentially expressed proteins in the G7D group and in the blue module.

(B) Venn diagram of differentially expressed proteins in the G4W group and in the blue module.

(C) Venn diagram of differentially expressed proteins in the green module, turquoise module, and in the G3M group.

(D) Venn diagram of differentially expressed proteins in the purple module, brown module, and in the G1Y group.

Fig. S6. Weighted gene co-expression network analysis (WGCNA) of regulatory networks in the turquoise, brown, and purple modules.

The protein regulatory networks in the turquoise (A), brown (B), and purple (C) modules constructed by WGCNA are illustrated.

Supplementary Table S1. List of identified proteins in the proteome of *G. platifrons* gills.

Supplementary Table S2. Differentially expressed proteins identified in different groups.

Supplementary Table S3. Identified metabolites in the metabolome of *G. platifrons* gills.

Supplementary Table S4. Differential metabolites identified in different groups.

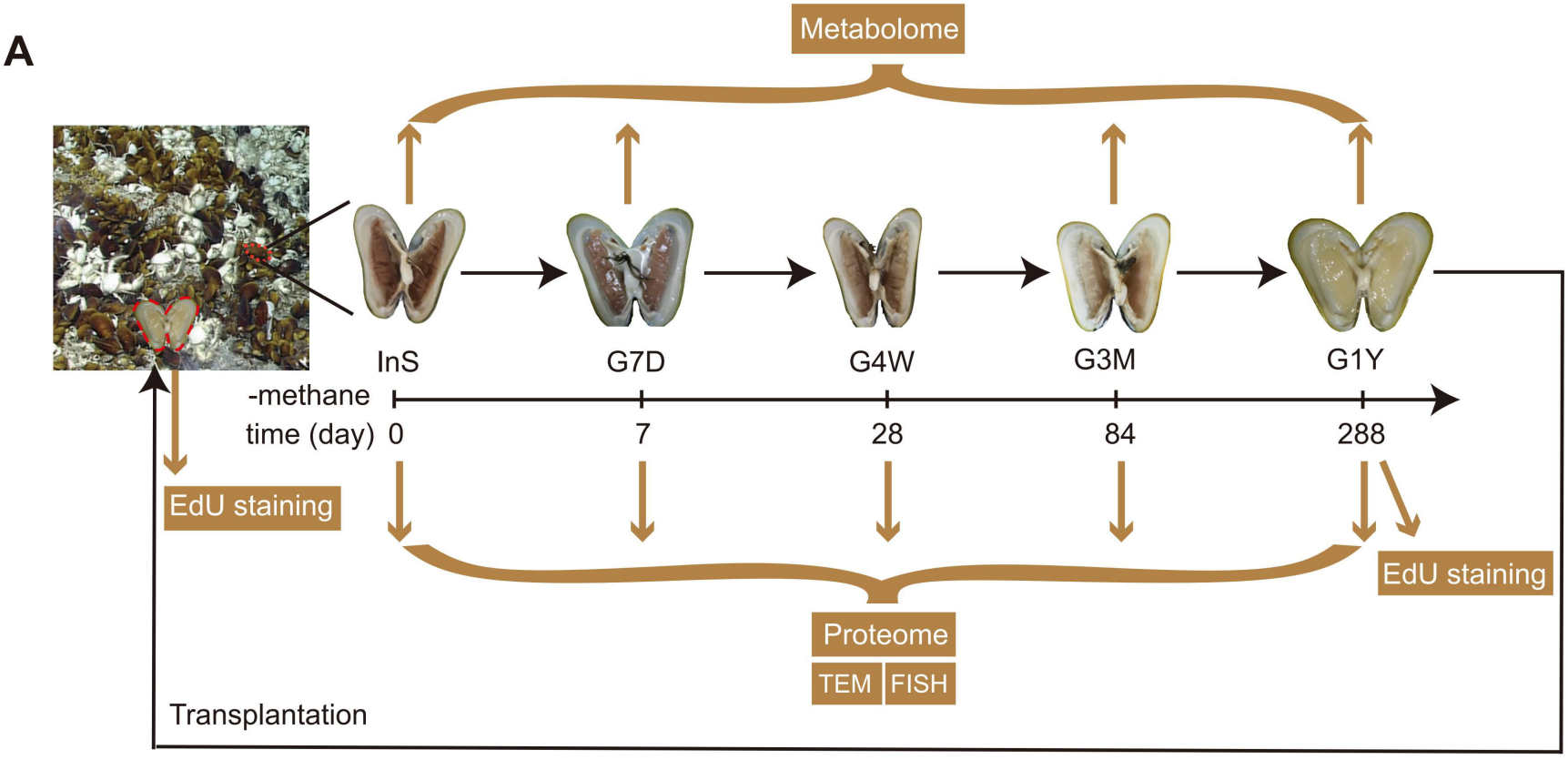
A
Metabolome
InS
G7D
G4W
G3M
G1Y
-methane
time (day)
0
7
28
84
288
EdU staining
EdU staining
Proteome
TEM
FISH
Transplantation

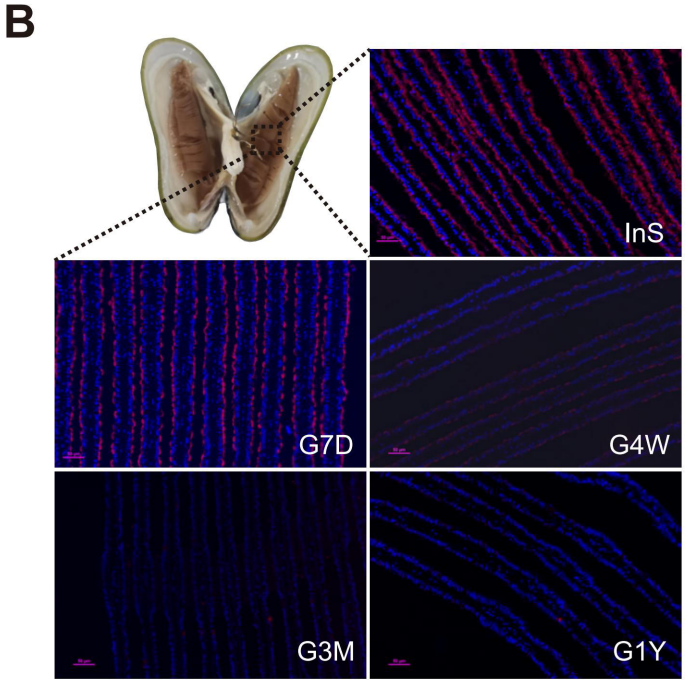
B
InS
G7D
G4W
G3M
G1Y

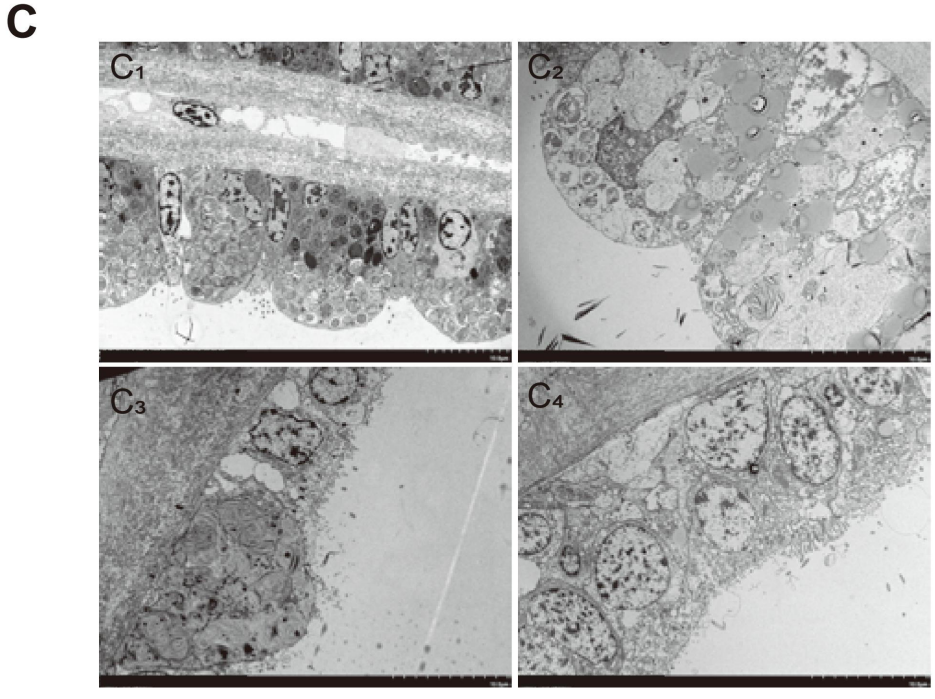
C
C1
C2
C3
C4

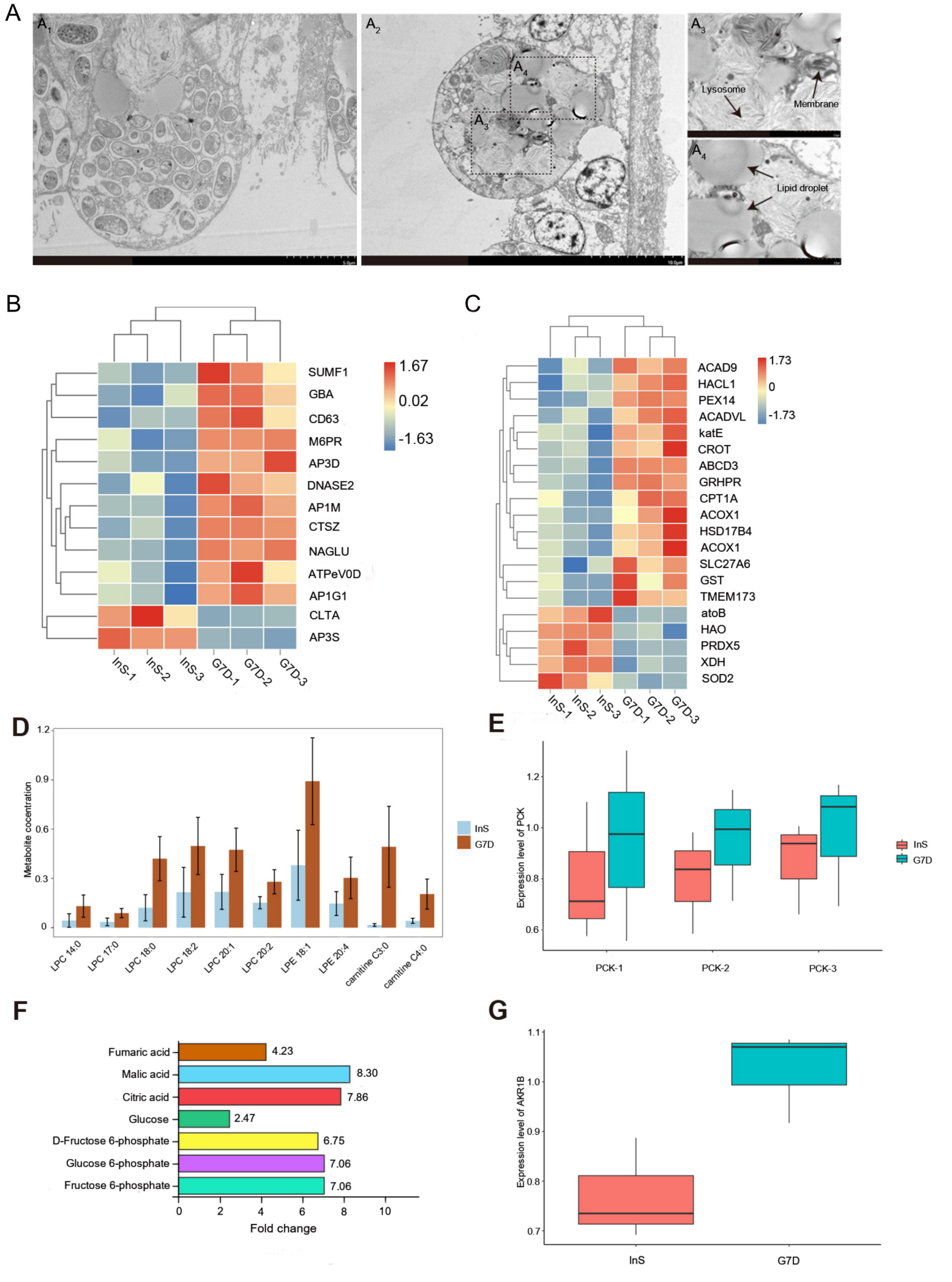
A
A1
A2
A3
A4
Lysosome
Membrane
Lipid droplet
B
SUMF1
GBA
CD63
M6PR
AP3D
DNASE2
AP1M
CTSZ
NAGLU
ATPeV0D
AP1G1
CLTA
AP3S
InS-1
InS-2
InS-3
G7D-1
G7D-2
G7D-3
1.67
0.02
-1.63
C
ACAD9
HACL1
PEX14
ACADVL
katE
CROT
ABCD3
GRHPR
CPT1A
ACOX1
HSD17B4
ACOX1
SLC27A6
GST
TMEM173
atoB
HAO
PRDX5
XDH
SOD2
1.73
0
-1.73
D
Metabolite cocentration
LPC 14:0
LPC 17:0
LPC 18:0
LPC 18:2
LPC 20:1
LPC 20:2
LPE 18:1
LPE 20:4
carnitine C3:0
carnitine C4:0
InS
G7D
E
Expression level of PCK
PCK-1
PCK-2
PCK-3
InS
G7D
F
Fumaric acid
Malic acid
Citric acid
Glucose
D-Fructose 6-phosphate
Glucose 6-phosphate
Fructose 6-phosphate
4.23
8.30
7.86
2.47
6.75
7.06
7.06
Fold change
G
Expression level of AKR1B
InS
G7D

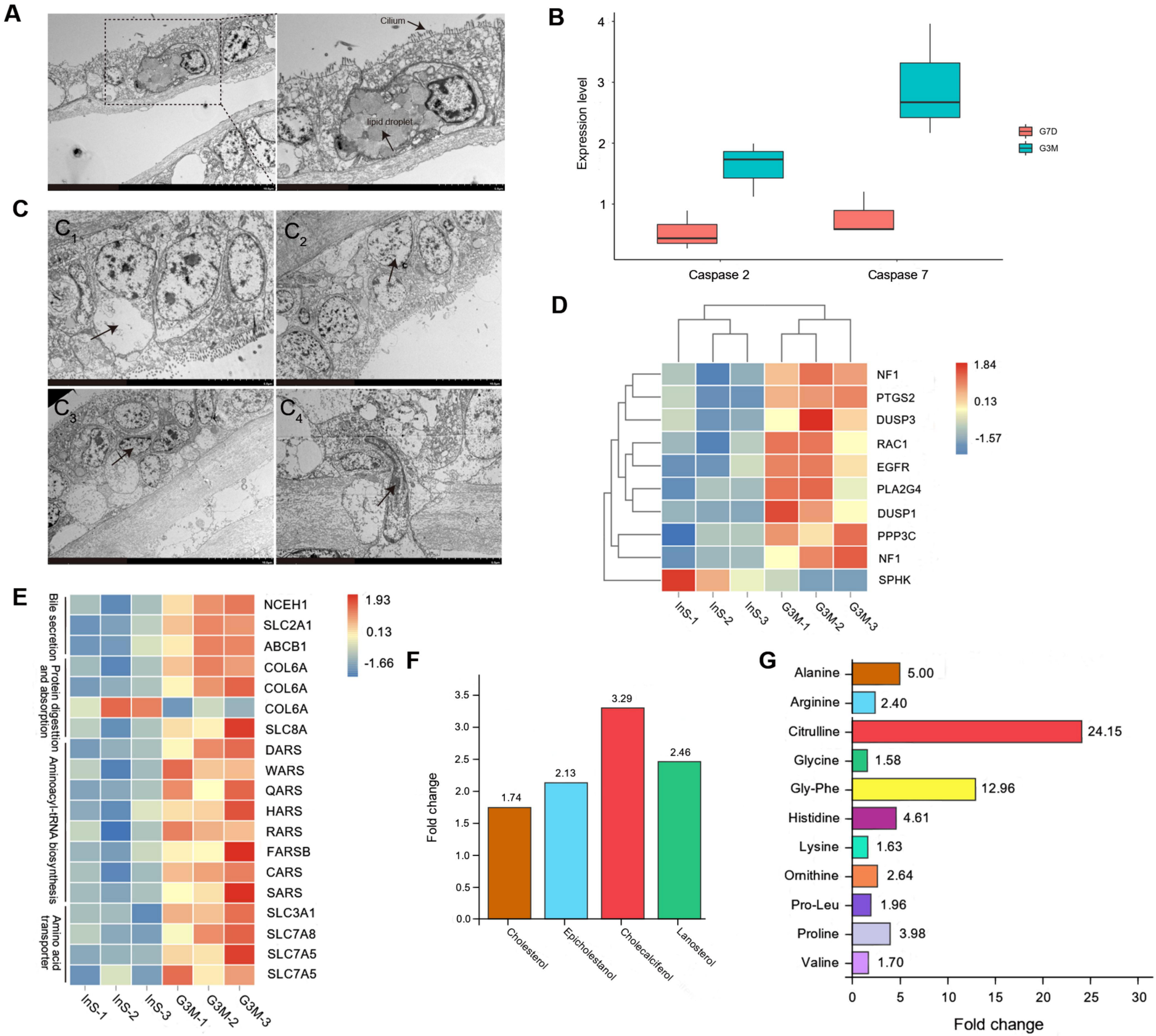
A
Cilium
lipid droplet
B
Expression level
4
3
2
1
Caspase 2
Caspase 7
G7D
G3M
C
C1
C2
C3
C4
D
NF1
PTGS2
DUSP3
RAC1
EGFR
PLA2G4
DUSP1
PPP3C
NF1
SPHK
InS-1
InS-2
InS-3
G3M-1
G3M-2
G3M-3
1.84
0.13
-1.57
E
Bile secretion
Protein digestion and absorption
Aminoacyl-tRNA biosynthesis
Amino acid transporter
NCEH1
SLC2A1
ABCB1
COL6A
COL6A
COL6A
SLC8A
DARS
WARS
QARS
HARS
RARS
FARSB
CARS
SARS
SLC3A1
SLC7A8
SLC7A5
SLC7A5
InS-1
InS-2
InS-3
G3M-1
G3M-2
G3M-3
1.93
0.13
-1.66
F
Fold change
3.5
3.0
2.5
2.0
1.5
1.0
0.5
0.0
1.74
2.13
3.29
2.46
Cholesterol
Epicholestanol
Cholecalciferol
Lanosterol
G
Alanine 5.00
Arginine 2.40
Citrulline 24.15
Glycine 1.58
Gly-Phe 12.96
Histidine 4.61
Lysine 1.63
Ornithine 2.64
Pro-Leu 1.96
Proline 3.98
Valine 1.70
0
5
10
15
20
25
30
Fold change

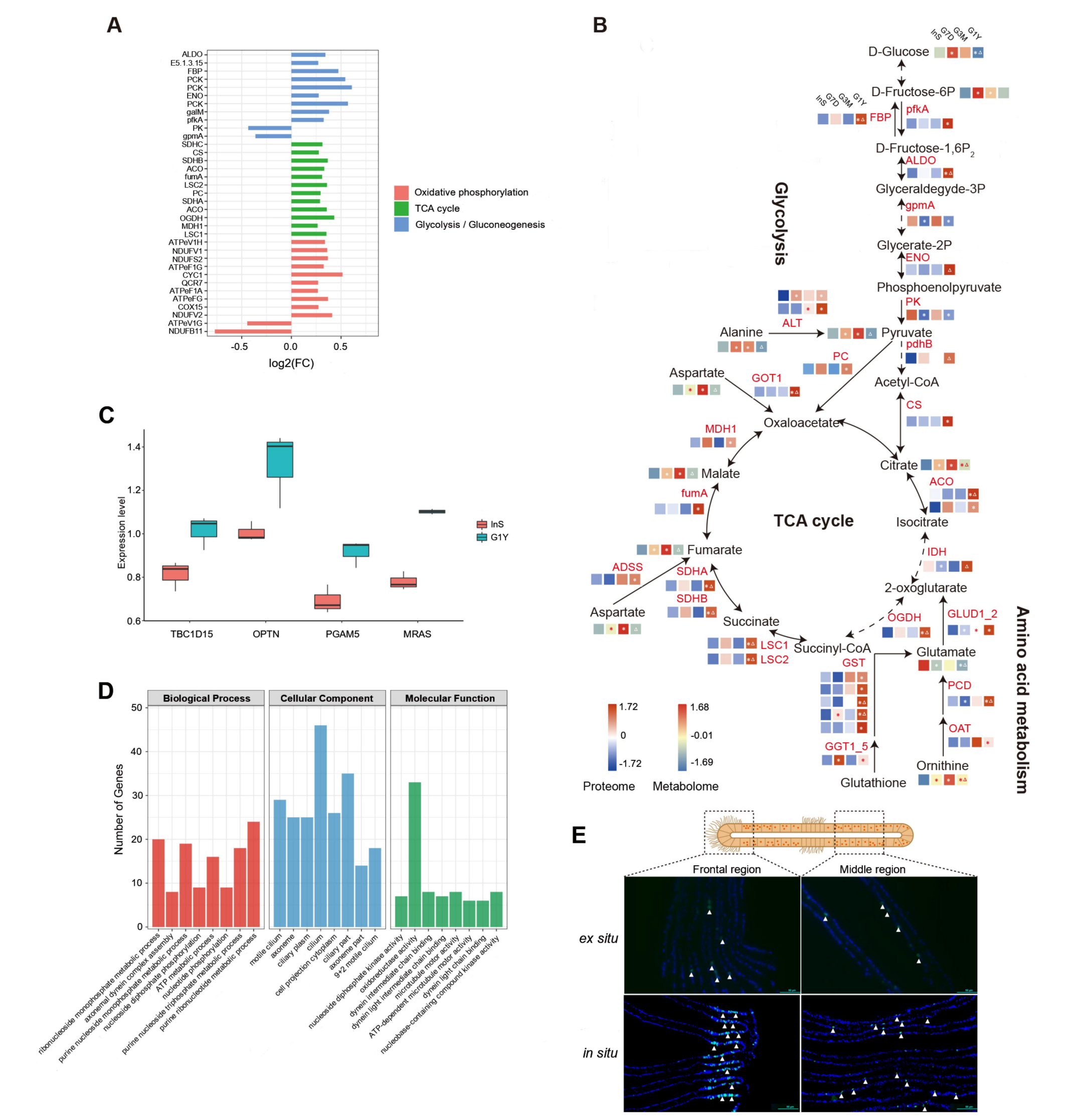
A
ALDO
E5.1.3.15
FBP
PCK
PCK
ENO
PCK
galM
pfkA
PK
gpmA
SDHC
CS
SDHB
ACO
fumA
LSC2
PC
SDHA
ACO
OGDH
MDH1
LSC1
ATPeV1H
NDUFV1
NDUFS2
ATPeF1G
CYC1
QCR7
ATPeF1A
ATPeFG
COX15
NDUFV2
ATPeV1G
NDUFB11
-0.5
0.0
0.5
log2(FC)
Oxidative phosphorylation
TCA cycle
Glycolysis / Gluconeogenesis
B
D-Glucose
D-Fructose-6P
FBP
pfkA
D-Fructose-1,6P2
ALDO
Glycolysis
Glyceraldegyde-3P
gpmA
Glycerate-2P
ENO
Phosphoenolpyruvate
PK
ALT
Alanine
Pyruvate
pdhB
PC
Aspartate
GOT1
Acetyl-CoA
CS
Oxaloacetate
MDH1
Citrate
Malate
ACO
fumA
TCA cycle
Isocitrate
Fumarate
IDH
ADSS
SDHA
2-oxoglutarate
SDHB
Aspartate
Succinate
OGDH
GLUD1_2
LSC1
LSC2
Succinyl-CoA
Glutamate
GST
PCD
OAT
GGT1_5
Ornithine
Glutathione
Amino acid metabolism
1.72
0
-1.72
Proteome
1.68
-0.01
-1.69
Metabolome
C
Expression level
1.4
1.2
1.0
0.8
0.6
TBC1D15
OPTN
PGAM5
MRAS
InS
G1Y
D
Biological Process
Cellular Component
Molecular Function
Number of Genes
50
40
30
20
10
0
ribonucleoside monophosphate metabolic process
axonemal dynein complex assembly
purine nucleoside monophosphate metabolic process
nucleoside diphosphate phosphorylation
ATP metabolic process
nucleotide phosphorylation
purine nucleoside triphosphate metabolic process
purine ribonucleotide metabolic process
motile cilium
axoneme
ciliary plasm
cilium
cell projection cytoplasm
ciliary part
axoneme part
9+2 motile cilium
nucleoside diphosphate kinase activity
oxidoreductase activity
dynein intermediate chain binding
dynein light intermediate chain binding
microtubule motor activity
ATP-dependent microtubule motor activity
dynein light chain binding
nucleobase-containing compound kinase activity
E
Frontal region
Middle region
ex situ
in situ

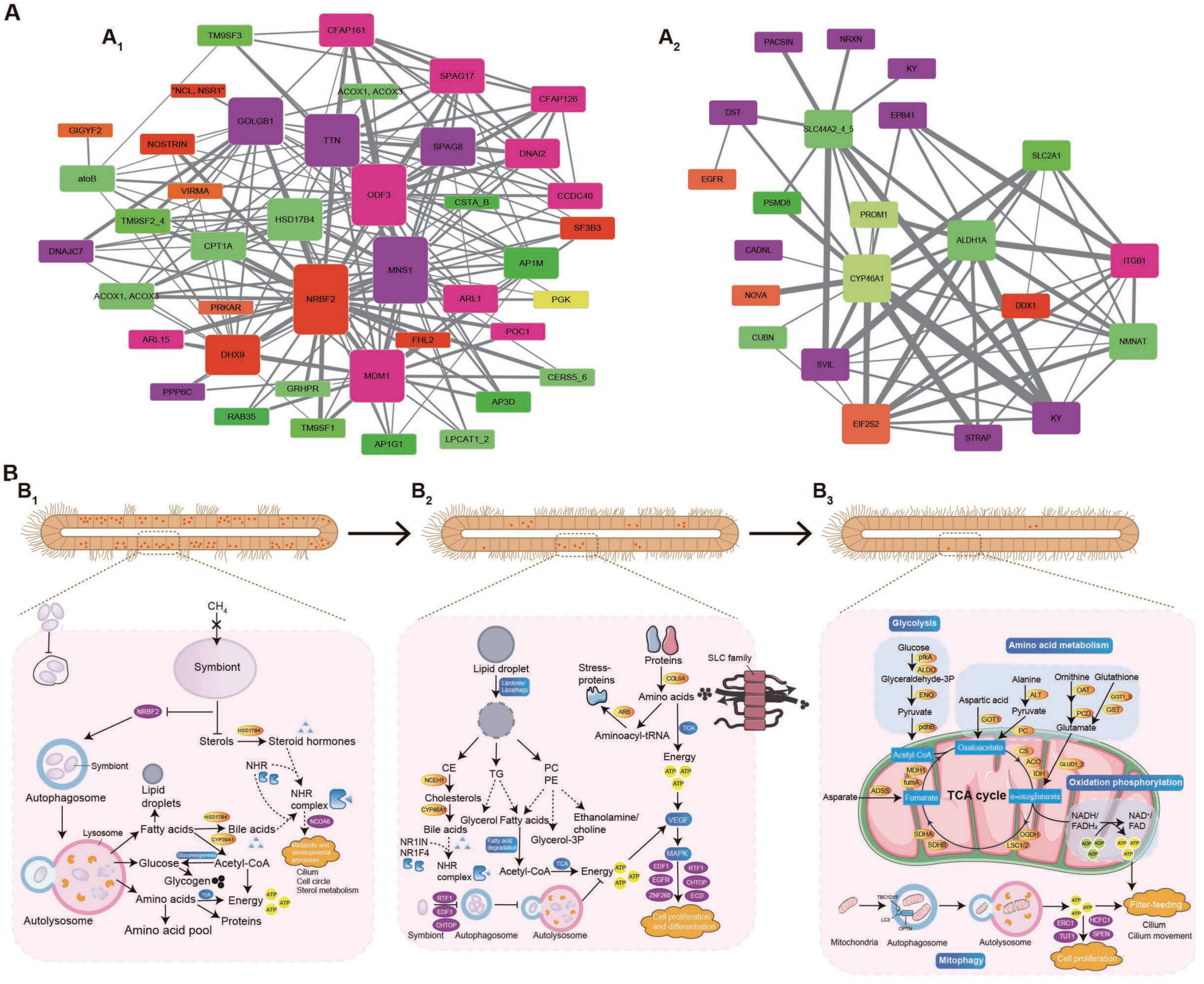
A
A1
TM9SF3
CFAP161
SPAG17
"NCL, NSR1"
ACOX1, ACOX3
CFAP126
GOLGB1
GIGYF2
NOSTRIN
TTN
SPAG8
DNAI2
atoB
VIRMA
ODF3
CCDC40
CSTA_B
TM9SF2_4
HSD17B4
SF3B3
DNAJC7
CPT1A
MNS1
AP1M
ACOX1, ACOX3
NRBF2
ARL1
PGK
PRKAR
ARL15
POC1
FHL2
DHX9
MDM1
CERS5_6
PPP6C
GRHPR
AP3D
RAB35
TM9SF1
AP1G1
LPCAT1_2
A2
PACSIN
NRXN
KY
DST
SLC44A2_4_5
EPB41
SLC2A1
EGFR
PSMD8
PROM1
ALDH1A
CADNL
ITGB1
CYP46A1
NOVA
DDX1
CUBN
NMNAT
SVIL
EIF2S2
KY
STRAP
B
B1
B2
B3
CH4
Symbiont
NRBF2
Sterols
HSD17B4
Steroid hormones
Symbiont
Autophagosome
Lipid droplets
NHR
NHR complex
NCOA6
Lysosome
Fatty acids
HSD17B4
Bile acids
CYP39A1
Metabolic and developmental processes
Glucose
Gluconeogenesis
Acetyl-CoA
Cilium
Cell circle
Sterol metabolism
Glycogen
Amino acids
TCA
Energy
ATP
Proteins
Autolysosome
Amino acid pool
Lipid droplet
Lipolysis/Lipophagy
Stress-proteins
Proteins
COL6A
SLC family
Amino acids
ARS
Aminoacyl-tRNA
TCA
Energy
CE
TG
PC
PE
NCEH1
Cholesterols
CYP46A1
Glycerol
Fatty acids
Ethanolamine/choline
Bile acids
Fatty acid degradation
Glycerol-3P
NR1IN
NR1F4
NHR complex
Acetyl-CoA
TCA
Energy
VEGF
MAPK
EDF1
RTF1
EGFR
CHTOP
ZNF260
ECD
Cell proliferation and differentiation
RTF1
EDF1
CHTOP
Symbiont
Autophagosome
Autolysosome
Glycolysis
Glucose
pfkA
ALDO
Glyceraldehyde-3P
ENO
Pyruvate
pdhB
Amino acid metabolism
Alanine
ALT
Ornithine
Glutathione
OAT
GGT1_5
GST
Aspartic acid
GOT1
Pyruvate
PCD
Glutamate
PC
Acetyl-CoA
Oxaloacetate
CS
ACO
IDH
GLUD1_2
MDH1
fumA
Asparate
ADSS
Fumarate
TCA cycle
α-oxoglutarate
Oxidation phosphorylation
NADH/FADH2
NAD+/FAD
SDHA
SDHB
OGDH
LSC1/2
ADP
ATP
Mitochondria
TBC1D15
LC3
OPTN
Autophagosome
Autolysosome
ERC1
TUT1
HCFC1
SPEN
Filter-feeding
Cilium
Cilium movement
Cell proliferation
Mitophagy